Advances in Nano Research, *Vol. 8 No. 2 (2020) 103-114*
DOI: https://doi.org/10.12989/anr.2020.8.2.103

Effect of laminate configuration on the free vibration/buckling of FG Graphene/PMMA composites

Mehran Karimi Zeverdejani [1] and Yaghoub Tadi Beni*[2,3]

[1] *Department of Mechanical Engineering, Shahrekord University, Shahrekord, Iran*
[2] *Faculty of Engineering, Shahrekord University, Shahrekord, Iran*
[3] *Nanotechnology Research Center, Shahrekord University, Shahrekord, Iran*

(*Received June 3, 2019, Revised September 20, 2019, Accepted October 1, 2019*)

Abstract. In this research, buckling and free vibration of rectangular polymeric laminate reinforced by graphene sheets are investigated. Various patterns are considered for augmentation of each laminate. Critical buckling load is evaluated for different parameters, including boundary conditions, reinforcement pattern, loading regime, and laminate geometric states. Furthermore, vibration analysis is investigated for square laminate. Elastic properties of the composite are calculated using a combination of both molecular dynamics (MD) and the rule of mixture (MR). Kinematics of the plate is approximated based on the first shear deformation theory (FSDT). The current analysis is performed based on the energy method. For the numerical investigation, Ritz method is applied, and for shape functions, Chebyshev polynomials are utilized. It is found that the number of layers is effective on the buckling load and natural frequency of laminates which made from non-uniform layers.

Keywords: buckling; free vibration; FG-laminates; molecular dynamics; boundary conditions; Ritz method

1. Introduction

Today, applications of smart progressive material have been changed significantly in design and manufacturing of structures in different industries. For improve the efficiency of systems, advanced materials are used in both nano and macro scales (Akgöz and Civalek 2017, 2018, Ghobadi *et al*. 2019, Mehralian *et al*. 2016a, b, Tadi Beni 2016, Kheibari and Tadi Beni 2017, Mohtashami and Tadi Beni 2019). One particular type of these materials is composite reinforced by nanofillers which provide superior mechanical, chemical an electrical property (Zhang and Park 2018, 2019, Zheng *et al*. 2018a, b). In order to increase the efficiency of composite materials, it is more desirable to utilize a kind of matrix which has a low cost and high performance, simultaneously (Shen *et al*. 2017, Mohammadimehr *et al*. 2018, Tam *et al*. 1019). Polymeric laminates are one of the most widely used elements in the various industrials such as aerospace, maritime and automobile industries (Walter *et al*. 2016). These laminates subjected to applied load maybe have buckled and consequently, lose their performances. Therefore, study of buckling behavior of them is important (Nemeth 1986, Tadi and Mehralian 2017). On the beam and plane-like structures which are subjected to a compressive load, the buckling phenomenon occurs when the energy capacity of structures to be full and the body intends to shape change (Tadi *et al*. 2017). Indeed, the buckling state is the separation point between the static equilibrium and post-buckling path. In order to ensure the stability of structures, prediction of buckling behavior of them is particularly important for designers (Mehralian and Tadi Beni 2016, Huang and Atluri 1995, Alibeigi *et al*. 2018, Ebnali Samani and Tadi Beni 2018). Furthermore, resonance phenomenon may also occur in the plate, where it oscillates with large amplitude. In order to control the resonance of structures, free vibration analysis of them is necessary (Aydogdu 2014, Soleimani and Tadi Beni 2018, Besseghier *et al*. 2015, Tadi Beni *et al*. 2015). Today, functionally graded material (FGM) is one of the most used materials in various systems. In this type of material physical properties change along special direction (Dastjerdi and Akgöz 2018, Shojaeian and Tadi Beni 2015). Functionally graded reinforced laminates are one of the newest structures. They are made from layers that each of them has a specific volume fractions of fillers. According to distribution schema of the fillers across the thickness of laminates, several patterns are introduced for laminates configuration (Song *et al*. 2017). The simplest type is U-pattern which all the layers contain the same value of reinforcements. Another form is O-pattern. In this pattern both upper and bottom layers have a minimum value of fillers and by the move towards the mid-surface, amount of fillers increases, so that mid-layer has an extreme value of reinforcement. On the contrary, in the X-pattern, upper and bottom layers have a greatest value of fillers and by the move towards mid-layer, the amount of fillers belittles, so that mid-layer has a less amount of reinforcement. Graphene sheet (GS) and carbon nanotube (CNT) are the best nanofillers for polymeric matrix (Mittal *et al*. 2015). Actually, it can be said GS is the substance of carbon based nono-fillers such as CNT, graphite, fullerene, and graphene

*Corresponding author, Professor,
E-mail: Tadi@eng.sku.ac.ir

ISSN: 2287-237X (Print), 2287-2388 (Online)

oxide sheet (GO) (Jia *et al*. 2018, Kaushik and Majumder 2015, Rodriguez-Perez *et al*. 2017). GS is one of the thinner known materials which has 3.4 Angstroms thickness. It has superior properties compared to other nano-fillers which one can note to excellent surface contacts and reasonable cost (Kocman *et al*. 2014). Several investigations have shown that conventional micromechanical theories cannot present the real value of mechanical properties for polymeric nanocomposites. According to the complexity and price of the experimental procedure, Molecular dynamics (MD) simulation can be a suitable approach for calculation of the mechanical constant of materials (Jia and Qingsheng 2009). Based on the MD method, Han and Eliot (2007) determined the elastic properties of CNT reinforced polymer composites. Li *et al*. (2019) investigated mechanical properties of polymer composites reinforced by CNT and GS. Temperature-dependent mechanical properties of a polymeric composite reinforced by woven graphene were studied by Lin *et al*. (2017). They demonstrated MD results are dissimilar to the results generated by conventional mixture rule. Shiu and Tsai (2014) based on MD studied the mechanical properties of the graphene-based polymeric composite. They considered epoxy as matrix and also implemented GS, GO and graphene flakes for reinforcements. Recently, several studies have been conducted on the mechanical behavior of FG-laminates (Ebrahimi and Habibi 2017, Fan *et al*. 2019, Malekzadeh and Zarei 2014, Nguyen-Quang *et al*. 2018, Shen and Xiang 2018, Shen *et al*. 2018). Shen *et al*. (2017a, b) analyzed buckling, bending and vibration of FG-laminated. Kiani (2017) investigated buckling of rectangular FG-CNT laminates subjected to a non-uniform compression load. Karimi et al. studied buckling and post-buckling of defected FG graphene/PMMA composite (Karimi *et al*. 2019). The vibration of FG-CNT conical shell studied by Kiani *et al*. (2018b). They also investigated the vibration of FG-CNT skew cylindrical shells (Kiani *et al*. 2018a). Shen and Xiang (2019) studied buckling and post-buckling of cylindrical FG-GS laminated subjected to torsional loads. Mirzaei and Kiani (2016) studied the vibration of FG-CNT cylindrical laminates. They also investigated thermal buckling of FG-GS laminates (Mirzaei and Kiani 2017).

In the present work, the free vibration and buckling behavior of FG-GS polymeric laminates are explored. In structural stability analysis, boundary and physical conditions have a vital rule in the response of structures respected to external loads. The main purpose of this research is to investigate the critical load and natural frequency of functionally graded graphene/PMMA laminates with arbitrary boundary conditions. In addition to mechanical properties, it is revealed that boundary conditions have an influential effect on body stiffness. As a result, the effects of geometrical conditions are studied on buckling and vibration of rectangular laminates. In buckling analysis, composite laminates are subjected to uniaxial, biaxial and shear loads. Also, the effects of geometrical conditions are investigated on free vibration of square laminate. Polymethyl methacrylate (PMMA) is considered as a matrix. Elastic properties of graphene/PMMA composite are predicted by MD simulation. Considering that conventional mixture rule cannot present reasonable data for polymeric nano-composites, by inserting MD results into the rule of mixture, corrective factors are calibrated for the aforementioned composite. For dynamic analysis, Chebyshev-Ritz method is implemented. The Chebyshev shape functions are selected in such a way that the various boundary conditions be satisfied. Laminates are considered in three U, O and X-pattern configurations. Furthermore, the effect of the number of layers (N) is investigated. It is revealed that the number of layers is irrelevant on both buckling load and natural frequency of U-pattern laminates. Moreover, it is shown that in all of the boundary conditions, X-pattern presents higher natural frequency and buckling load compared to U-pattern. As well as, it is illustrated that in laminates with two free opposite edges, critical buckling loads are more close to each other for higher aspect ratios.

2. Laminate configurations

In the present study, there are two opinions to explore the influence of layers arrangement on the laminate configuration. The first view is the pattern of graphene distribution in layers. Accordingly, three patterns are considered including U-pattern, O-pattern, and X-pattern. Another view is the number of layers. It should be noted that in this study, volume fractions of reinforcement are identical in all of the samples. It is obvious that for the same volume fraction, number of layers could have an important role in body stiffness (Fig. 1). For each layer, the volume fraction of graphene is measured from the following formula

$$\begin{aligned} U &: \mathrm{V}_G(\mathrm{k}) = \mathrm{V}_G^* \\ O &: \mathrm{V}_G(\mathrm{k}) = 2\,\mathrm{V}_G^*\left(1-\left|(2k-N-1)/N\right|\right) \\ X &: \mathrm{V}_G(\mathrm{k}) = 2\,\mathrm{V}_G^*\left|(2k-N-1)/N\right| \end{aligned} \tag{1}$$

Where k represents the number of the corresponding layer, N signifies the total number of layers and V_G^* is also total graphene volume fraction in each laminate.

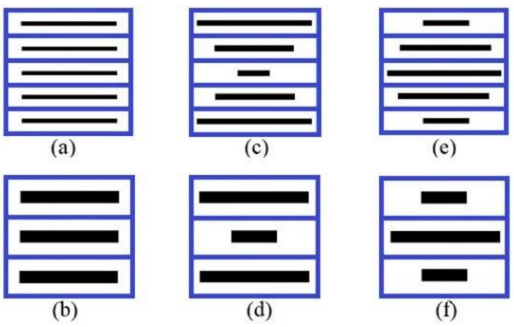

Fig. 1 Schematic of laminate section patterns: (a) U-pattern 5 layers; (b) U-pattern 3 layers; (c) X-pattern 5 layers; (d) X-pattern 3 layers; (e) O-pattern 5 layers; (f) O-pattern 3 layers

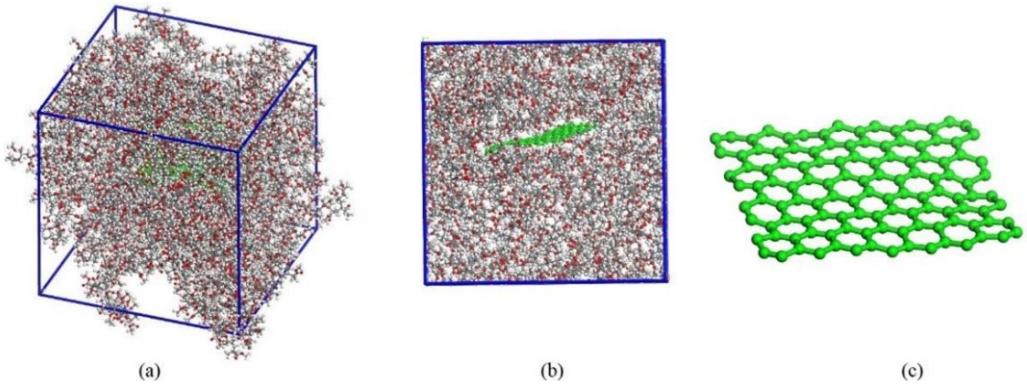

Fig. 2 Molecular model of (a) graphene/PMMA composite; (b) section view of composite; (c) graphene sheet

Table 1 Mechanical properties (*Gpa*) of graphene and PMMA

	Graphene						PMMA				
	E_x	E_y	G	υ	ρ		E_x	E_y	G	υ	ρ
Present work	1120	1134	235	0.41	2.33	Present work	3.12	3.33	1.08	0.34	1.14
Reddy *et al*. (2005)	1106-1201	-	288	0.44-0.46	-	Van Krevelen and Te Nijenhuis (2009)	3.2	-	1.10	0.4	1.17
Sakhaee-Pour (2009)	1040	-	213-233	1.12	-	Jaiganesh *et al*. (2015)	3.3	-	1.7	0.38-0.4	1.19

Table 2 Mechanical properties and corrective factors graphene/PMMA composite

	wt	V_G	$E_{Composite}$	$G_{Composite}$	η_1	η_2
Ramanathan *et al*. (2007)	0.02	0.0098	3.70	-	0.057	-
	0.05	0.0249	4.70	-	0.060	-
Current study (MD)	0.05	0.0249	4.45	1.44	0.051	1.30
	0.07	0.0352	5.40	1.59	0.061	1.42
	0.10	0.0494	6.10	1.66	0.055	1.46
	0.12	0.0620	6.82	1.70	0.056	1.48

3. Elastic properties of the composite

To determine the elastic properties of graphene/PMMA composite, molecular dynamic simulation is implemented. After modeling all of the components, the mechanical properties of each of them are measured which they have a good agreement with results coming in the literature (Jaiganesh *et al*. 2015, Reddy *et al*. 2005, Sakhaee-Pour 2009, Van Krevelen and Te Nijenhuis 2009).

The schematic of molecular models is presented in Fig. 2. In this simulation COMPASS force-field is used (Chen *et al*. 2018). After optimization of the molecular model, the composite is subjected to the NVT ensemble with 500°C temperature for 100 picoseconds. Then, it is subjected to the NPT ensemble with 298°C temperature and 0.1 *Gpa* pressure for 100 picoseconds. After energy minimizing, by applying constant strain on the molecular model, the shear and Young's moduli of the graphene/PMMA composite are obtained for different values of fillers (Table 2). In the present MD simulation, Graphene weight fractions (wt) is set equal to 0.05, 0.07, 0.10 and 0.12. It is revealed that for 0.05 weight fraction of graphene, young modulus obtained from MD simulations (4.45) is predicted close to experimental data (4.7) (Ramanathan *et al*. 2007). It should be noted that due to a huge gap between graphene and PMMA elastic moduli, conventional mixture rule cannot predict the reasonable amounts of composite properties. For this reason, in order to improve the accuracy of this theory, corrective factors namely η_1 and η_2 are defined which η_1 is related to in-plane Young's moduli and η_2 is related to the shear modulus.

$$E_{xx} = E_{yy} = \eta_1 V_G E_G + V_{PMMA} E_{PMMA}$$
$$\frac{\eta_2}{G} = \frac{V_G}{G_G} + \frac{V_{PMMA}}{G_{PMMA}} \tag{2}$$

It has been shown that in order to evaluation of the poison's ratio and density of laminates, one can use the simple form of mixture rule.

$$\nu_{xy} = \nu_{yx} = V_G \nu_G + V_{PMMA} \nu_{PMMA} \tag{3}$$

$$\rho = V_G \rho_G + V_{PMMA} \rho_{PMMA} \tag{4}$$

By inserting the results provided from MD simulation into the above equations, η_1 and η_2 coefficients are calibrated for Graphene/PMMA composite. It is shown that η_1 coefficient resulting from the present study is in the range of η_1 related to experimental data (Table 2).

4. Problem formulation

In order to extract the critical buckling load and natural frequency, one can use of energy method. In this work, numerical analysis is conducted based on the Ritz method (Emdadi *et al*. 2019). According to this approach, the total energy of a body is defined as follows

$$\Pi = U - W_{ext} - K \tag{5}$$

Where U, W_{ext} and K are laminate strain energy, the work done by external loads and laminate kinetic energy, respectively. Strain energy is a function of stress and strain tensors. Kinetic energy arises from the below equation.

$$U = \frac{1}{2}\int_V \sigma_{ij}\varepsilon_{ij}\, dV \tag{6}$$

$$\begin{aligned} K = \frac{1}{2}\iint_A \Bigg[& I_1\left(\frac{\partial u}{\partial t}^2 + \frac{\partial v}{\partial t}^2 + \frac{\partial w}{\partial t}^2\right) \\ & + I_2\left(\frac{\partial u}{\partial t}\frac{\partial \theta_x}{\partial t} + \frac{\partial v}{\partial t}\frac{\partial \theta_y}{\partial t}\right) \\ & + I_3\left(\frac{\partial \theta_x}{\partial t}^2 + \frac{\partial \theta_y}{\partial t}^2\right)\Bigg] dxdy \end{aligned} \tag{7}$$

Which I_i are mass inertia terms which are defined as

$$\begin{pmatrix} I_1 \\ I_2 \\ I_3 \end{pmatrix} = \sum_{k=1}^{N} \rho_{(k)} \begin{pmatrix} z_{(k+1)} - z_{(k)} \\ \frac{1}{2}\left[{z_{(k+1)}}^2 - {z_{(k)}}^2\right] \\ \frac{1}{3}\left[{z_{(k+1)}}^3 - {z_{(k)}}^3\right] \end{pmatrix} \tag{8}$$

Where $z_{(k)}$ and $z_{(k+1)}$ are the heights of the bottom and top of *k-th* layer. Moreover, $\rho_{(k)}$ is the density of *k-th* layer. For general loading, external work arises from following equation.

$$\begin{aligned} W_{ext} = \frac{1}{2}\int_V \Bigg[& N_{xx}^0\left(\frac{\partial w}{\partial x}\right)^2 + N_{yy}^0\left(\frac{\partial w}{\partial y}\right)^2 \\ & + 2N_{xy}^0\left(\frac{\partial w}{\partial x}\right)\left(\frac{\partial w}{\partial y}\right)\Bigg] dV \end{aligned} \tag{9}$$

Where ${N_{xx}}^0$ and ${N_{yy}}^0$ represent the axial loads in the X and Y-directions, respectively. Moreover, ${N_{xy}}^0$ is shear load (Fig. 3). The intensity of distributed stress on plate domain has a vital role in buckling analysis. According to applying the uniform loads in the laminate edges, the distribution of in-plane stress in the laminate is equal to applied loads on the edges (Kiani 2017). For orthotropic behavior, stress-strain relationships are expressed in the following matrix form

$$\begin{Bmatrix} \sigma_{xx} \\ \sigma_{yy} \\ \sigma_{zy} \\ \sigma_{xz} \\ \sigma_{xy} \end{Bmatrix} = \begin{bmatrix} Q_{11} & Q_{12} & 0 & 0 & 0 \\ Q_{21} & Q_{22} & 0 & 0 & 0 \\ 0 & 0 & Q_{44} & 0 & 0 \\ 0 & 0 & 0 & Q_{55} & 0 \\ 0 & 0 & 0 & 0 & Q_{66} \end{bmatrix} \begin{Bmatrix} \varepsilon_{xx} \\ \varepsilon_{yy} \\ \gamma_{zy} \\ \gamma_{xz} \\ \gamma_{xy} \end{Bmatrix} \tag{10}$$

That Q_{ij}'s are components of stiffness matrix which for each layer are defined as follows

$$\begin{aligned} & Q_{11}^{(k)} = \frac{E_{xx}^{(k)}}{\left(1 - \nu_{xy}\nu_{xy}\right)}, \quad Q_{22}^{(k)} = \frac{E_{yy}^{(k)}}{\left(1 - \nu_{xy}\nu_{xy}\right)} \\ & Q_{12}^{(k)} = Q_{21}^{(k)} = \frac{\nu_{xy}E_{xx}^{(k)}}{\left(1 - \nu_{xy}\nu_{xy}\right)} \\ & Q_{44}^{(k)} = G_{yz}^{(k)}, \quad Q_{55}^{(k)} = G_{xz}^{(k)}, \quad Q_{66}^{(k)} = G_{xy}^{(k)} \end{aligned} \tag{11}$$

Where E_{ij} and G_{ij} are young and shear moduli. Also, υ_{ij} represents the poison's ratio. Besides, strain components are defined as follows

$$\begin{aligned} & \varepsilon_{xx} = \frac{\partial u}{\partial x}, \quad \varepsilon_{yy} = \frac{\partial v}{\partial x}, \quad \gamma_{zy} = \frac{\partial v}{\partial z} + \frac{\partial w}{\partial y} \\ & \gamma_{xz} = \frac{\partial u}{\partial z} + \frac{\partial w}{\partial x}, \quad \gamma_{xy} = \frac{\partial u}{\partial y} + \frac{\partial v}{\partial x} \end{aligned} \tag{12}$$

Where u, v and w represents displacement components in X, Y, and Z directions, respectively. According to the FSDT model, displacement of each point in the body domain may be defined as the following form

$$\begin{aligned} & u = u_0(x,y,t) + z\theta_x(x,y,t) \\ & v = v_0(x,y,t) + z\theta_y(x,y,t) \\ & w = w_0(x,y,t) \end{aligned} \tag{13}$$

Where u_0, v_0, and w_0 are mid-plane dislocations in X, Y, and Z -axis, respectively. θ_x and θ_y are also rotation around Y and X-axis. By inserting Eqs. (6)-(13) into Eq. (5), one can write

$$\begin{aligned} \Pi = \frac{1}{2}\int_{-a/2}^{a/2}\int_{-b/2}^{b/2} \Bigg[& \sum_{k=1}^{N} \Bigg\{ A_{11}^{(k)} u_{0,x}^2 + D_{11}^{(k)} \theta_{x,x}^2 \\ & + A_{22}^{(k)} v_{0,\mathrm{y}}^2 + D_{22}^{(k)} \theta_{\mathrm{y},\mathrm{y}}^2 + 2B_{22}^{(k)} v_{0,\mathrm{y}} \theta_{\mathrm{y},x} + A_{55}^{(k)} \theta_{\mathrm{x}}^2 \\ & + 2A_{12}^{(k)} u_{0,x} v_{0,\mathrm{y}} + 2B_{12}^{(k)} \theta_{y,y} u_{0,x} + 2B_{12}^{(k)} v_{0,\mathrm{y}} \theta_{x,x} \\ & + 2D_{12}^{(k)} \theta_{x,x} \theta_{y,y} + A_{66}^{(k)} u_{0,\mathrm{y}}^2 + A_{66}^{(k)} v_{0,x}^2 \\ & + D_{66}^{(k)} \theta_{\mathrm{y},x}^2 + 2B_{66}^{(k)} u_{0,\mathrm{y}} \theta_{x,\mathrm{y}} + 2B_{66}^{(k)} u_{0,\mathrm{y}} \theta_{\mathrm{y},\mathrm{x}} \\ & + 2A_{66}^{(k)} u_{0,\mathrm{y}} v_{0,x} + 2B_{66}^{(k)} v_{0,\mathrm{x}} \theta_{x,\mathrm{y}} + 2B_{66}^{(k)} v_{0,\mathrm{x}} \theta_{y,x} \\ & + A_{55}^{(k)} w_{0,x}^2 + 2D_{66}^{(k)} \theta_{x,\mathrm{y}} \theta_{y,x} + 2A_{55}^{(k)} w_{0,x} \theta_x \\ & + A_{44}^{(k)} w_{0,\mathrm{y}}^2 + 2A_{44}^{(k)} w_{0,\mathrm{y}} \theta_y + A_{44}^{(k)} \theta_y^2 + D_{66}^{(k)} \theta_{x,\mathrm{y}}^2 \\ & + 2B_{11}^{(k)} u_{0,x} \theta_{x,x} - I_1\left(\frac{\partial u}{\partial t}^2 + \frac{\partial v}{\partial t}^2 + \frac{\partial w}{\partial t}^2\right) \end{aligned} \tag{14}$$

$$-I_2\left(\frac{\partial u}{\partial t}\frac{\partial \theta_x}{\partial t}+\frac{\partial v}{\partial t}\frac{\partial \theta_y}{\partial t}\right)-I_3\left(\frac{\partial \theta_x}{\partial t}^2+\frac{\partial \theta_y}{\partial t}^2\right)\Bigg\} \\ -N_{xx}^0 w_{0,x}^2-2N_{xy}^0 w_{0,x}w_{0,y}-N_{yy}^0 w_{0,y}^2 dxdy\Bigg]dxdy \tag{14}$$

In the above equation, A_{ij} is stretching stiffness matrix, B_{ij} indicates bending-stretching matrix and D_{ij} represents bending stiffness matrix which they are defined as follows

$$A_{ij}^{(k)}=Q_{ij}^{(k)}\left[z_{(k+1)}-z_{(k)}\right] \\ B_{ij}^{(k)}=\frac{1}{2}Q_{ij}^{(k)}\left[z_{(k+1)}^2-z_{(k)}^2\right] \\ D_{ij}^{(k)}=\frac{1}{3}Q_{ij}^{(k)}\left[z_{(k+1)}^3-z_{(k)}^3\right] \tag{15}$$

According to Chebyshev-Ritz method, the components of displacement variables are defined as follows

$$u_0=R^u e^{i\omega t}\sum_{i=1}^{n}\sum_{j=1}^{m}T_{ij}^u p_{ij}(x,y) \\ v_0=R^v e^{i\omega t}\sum_{i=1}^{n}\sum_{j=1}^{m}T_{ij}^v p_{ij}(x,y) \\ w_0=R^w e^{i\omega t}\sum_{i=1}^{n}\sum_{j=1}^{m}T_{ij}^w p_{ij}(x,y) \\ \theta_x=R^{\theta_x} e^{i\omega t}\sum_{i=1}^{n}\sum_{j=1}^{m}T_{ij}^{\theta_x} p_{ij}(x,y) \\ \theta_y=R^{\theta_y} e^{i\omega t}\sum_{i=1}^{n}\sum_{j=1}^{m}T_{ij}^{\theta_y} p_{ij}(x,y) \tag{16}$$

Which, R^α and T_{ij}^α ($\alpha = u, v, w, \theta_x, \theta_y$) represent the auxiliary functions and unknown amplitudes, respectively. ω is also natural frequency of laminate. n and m are the numbers of Chebyshev approximation function in X and Y-direction. As well as, p_{ij} is the in-plane Chebyshev function which is defined as follows

$$p_{ij}(x,y)=\left(\cos\left[(i-1)\,arccos(\frac{2x}{a})\right]\right) \\ \left(\cos\left[(j-1)\,arccos(\frac{2y}{b})\right]\right) \tag{17}$$

As you know, in the Ritz method shape functions must satisfy the essential boundary conditions. Therefore, auxiliary functions R^α must be chosen in the way that boundary conditions to be established. In this study, several boundary conditions are considered. It should be noted that in buckling analysis, clamped and simply supported boundaries are allowable for in-plane displacement (in-plane movable boundary). While, in free vibration analysis clamped and simply supported boundaries are constrained (in-plane immovable boundary). For example, for laminate with CSCS boundary condition, the auxiliary functions for buckling analysis selected as follows

$$R^x=R^y=1, R^{\theta_y}=\left(1-\frac{2x}{a}\right)\left(1+\frac{2x}{a}\right) \\ R^w=R^{\theta_x}=\left(1-\frac{2x}{a}\right)\left(1+\frac{2x}{a}\right)\left(1-\frac{2y}{b}\right)\left(1+\frac{2y}{b}\right) \tag{18}$$

While, for free vibration analysis auxiliary functions are consider as follows

$$R^x=\left(1-\frac{2x}{a}\right)\left(1+\frac{2x}{a}\right)\left(1-\frac{2y}{b}\right)\left(1+\frac{2y}{b}\right) \\ R^x=R^y=R^w=R^{\theta_x}, R^{\theta_y}=\left(1-\frac{2x}{a}\right)\left(1+\frac{2x}{a}\right) \tag{19}$$

In order to minimize the total energy, derivation of energy function Π respected to amplitude parameters (T_{ij}^α) should be equal to zero, which cause to produce $5\times n\times m$ equations.

$$\frac{\partial \Pi}{\partial T_{ij}^\alpha}=0 \tag{20}$$

It should be noted, regardless of terms corresponded to kinetic energy, energy function will be calculate for buckling analysis, and by omitting the external loads, energy function will be set for free vibration analysis. Finally, following Eigen value problems are created.

$$[K_L]\{T_{ij}^\alpha\}=\{N_{cr}\}[K_g]\{T_{ij}^\alpha\} \tag{21}$$

$$[K_L]\{T_{ij}^\alpha\}=\{\omega^2\}[M]\{T_{ij}^\alpha\} \tag{22}$$

In this equations K_L is the linear stiffness of laminate, K_g represents geometrical stiffness matrix and M is mass stiffness matrix. Also, N_{cr} and ω^2 denote Eigen value. By solving Eqs. (21) and (22), the critical buckling load and square of laminate natural frequency can be obtained.

5. Results and discussions

In this section, numerical results are presented for critical buckling load and natural frequency of the Graphene/PMMA laminates. First, the critical buckling load is investigated. Uniform and biaxial compression in addition to shear loads are applied to laminates. Several boundary conditions are considered for laminate. Each of them is introduced by four letters, which from left to right are corresponded to x = -a/2, y = -b/2, x = a/2, and y = b/2 boundaries. All of the boundary conditions are demonstrated by special symbols which made from three letters C, S, and F which represents clamped, simply supported and free edges, respectively. For instance, CSCS related to the laminate with simply support edges in y = ±b/2 and clamped edges in x = ±a/2. For the comparison study, thin isotropic steel plates with simply supported boundary conditions are considered. In the Table 3, the results obtained from the present solving method are compared with those of both FSDT and Kirchhoff (classic) plates (Sayyad and Ghugal 2014). In this table, non-dimensional critical load N_0 are presented for various thickness and side to length ratios (h/a, b/a). The number of

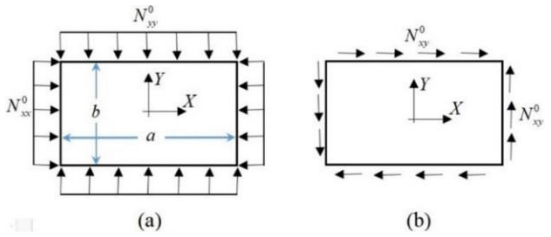

Fig. 3 Schematic of a laminate model subjected to various loads: (a) biaxial compression load; (b) shear load

Chebyshev function n and m are set equal to 8. As mentioned in the previous section, in this study kinematics of the laminated composite plate are considered according to FSDT model which provides accurate predictions for moderately thick plates. Indeed, the classic model does not have adequate sensitivity to laminate thickness.

As seen in Table 3, for thinner plates (a/h = 50) the results related to both classic and FSDT models are very close to each other, while for a/h = 20 and 10 there is a significant difference between aforementioned models.

Table 3 Comparison of buckling load ($N_0 = N_{cr}a^2/Eh^3$) for different geometrical ratios (b/a, a/h) for SSSS steel plate (b = 1m, E = 210 Gpa, v = 0.3, $G = E/2[1+v]$ Gpa)

a/h		b/a = 1		2		3	
		N_0	Error	N_0	Error	N_0	Error
10	Classic	3.6152	5.59%	1.4122	3.53%	1.1158	3.10%
	FSDT	3.4222	0.27%	1.3641	0.12%	1.0819	0.06%
	Present	3.4131	-	1.3624	-	1.0812	-
20	Classic	3.6152	1.53%	1.4122	0.94%	1.1158	0.82%
	FSDT	3.5649	0.14%	1.3999	0.07%	1.1071	0.04%
	Present	3.5600	-	1.3989	-	1.1067	-
50	Classic	3.6152	0.28%	1.4122	0.18%	1.1158	0.15%
	FSDT	3.6071	0.06%	1.4103	0.04%	1.1145	0.04%
	Present	3.6050	-	1.4097	-	1.1141	-

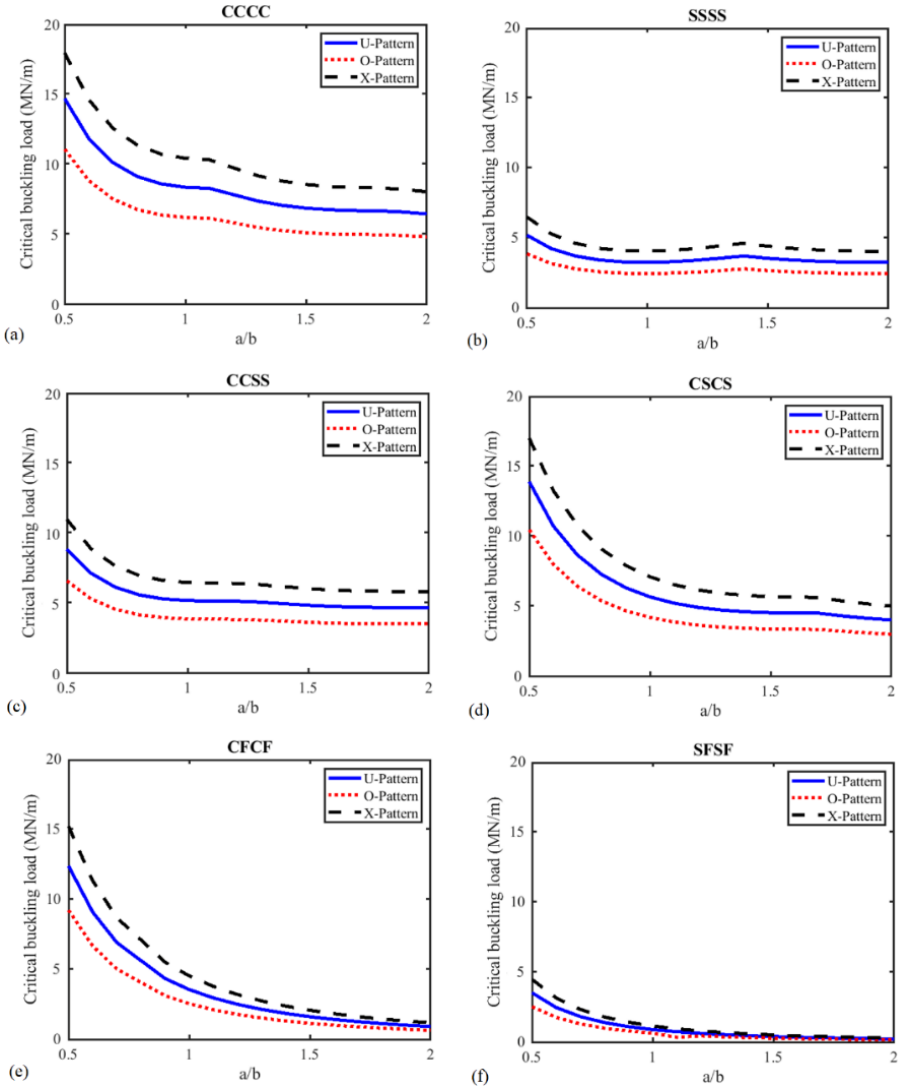

Fig. 4 Variation of uniaxial buckling load (MN/m) with aspect ratio for various laminate

Moreover, it is revealed that results obtained from present work have a good agreement by those of other FSDT simulation and maximum of errors is 0.27%.

In this section, a numerical study is considered for 0.1 total graphene volume fraction. The width to thickness (b/h) ratio of laminates is set equal to 20.

Furthermore, mechanical properties of each layer defined by advanced mixture rule, which corrective factors η_1 and η_2 are considered equal to 0.05 and 1.35, respectively. Fig. 4 presents the variation of critical buckling load respected to laminate aspect ratios (a/b) for uniaxial compression. In this section, the number of layers is considered equal to $N = 9$. Each of the graphs is related to special boundary conditions. It is obvious that in all of the boundary conditions, X-pattern laminate has provided higher buckling load compared to U-pattern. On the contrary, O-pattern laminate presents lower buckling load rather than U-pattern. Furthermore, it is clear that in CFCF and SFSF laminates for higher aspect ratios the effect of distribution pattern on the buckling load is less. As well as, by comparing the graphs, it has been clear that in all of the patterns, the minimum buckling load is related to SFSF and the maximum one happen for CCCC laminate. Also, it is revealed that CSCS treats near to the CCCC case for lower

Table 4 Critical buckling load (MN/m) for different layers number N

	U-Type			O-Type			X-Type		
N	3	5	9	3	5	9	3	5	9
SSSS	3.2458	3.2458	3.2458	2.7717	2.5414	2.4494	3.7189	3.9476	4.0388
CCCC	8.3327	8.3327	8.3327	7.0617	6.4254	6.1695	9.5700	10.1653	10.4010
CCSS	5.1503	5.1503	5.1503	4.3778	3.9901	3.8365	5.9180	6.2883	6.4355
CSCS	5.6491	5.6491	5.6491	4.7805	4.3520	4.1802	6.5039	6.9157	7.0792

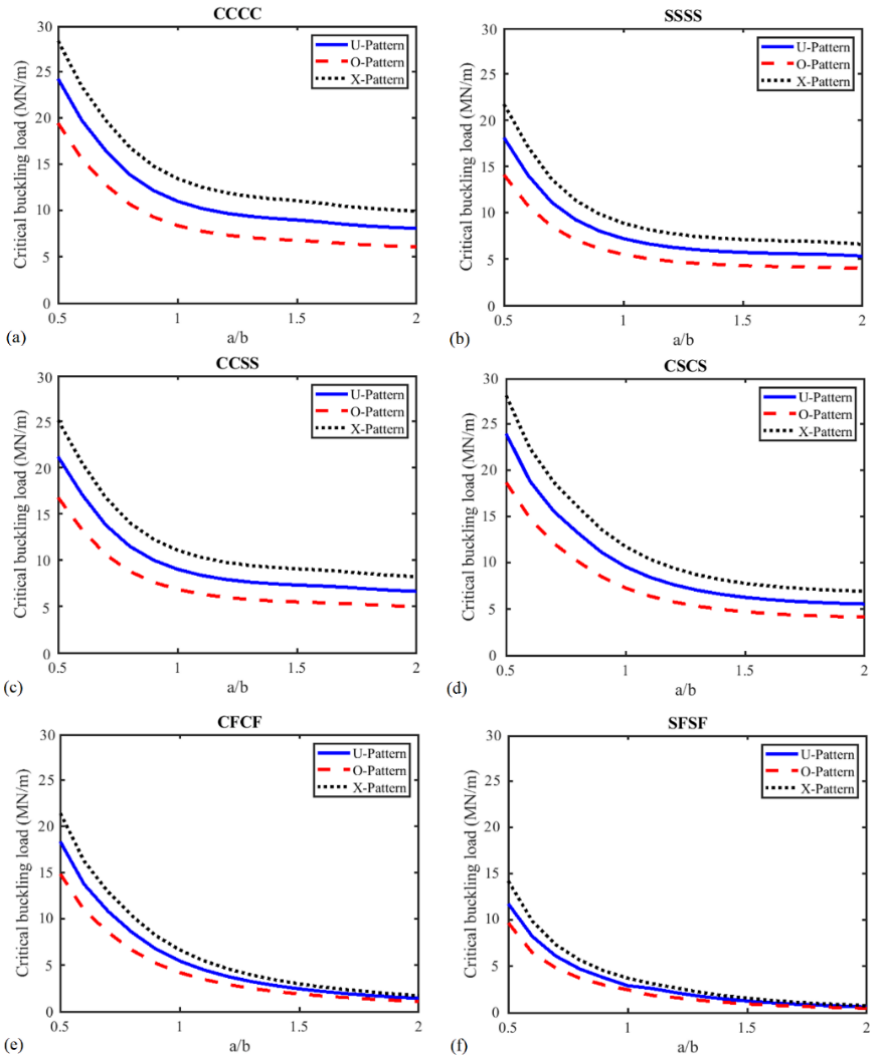

Fig. 5 Variation of shear buckling load (MN/m) with aspect ratio for various laminate configurations

aspect ratio, and behaves same to CCSS laminates in higher aspect ratio.

As mentioned in the introduction, the number of layers can affect the stiffness of laminates and it can change the critical loads. It is noted that in this section the total volume fraction of graphene is independent of layers number, and in all of the cases, total volume fraction is equal to 0.1. In Table 4, the buckling load is presented for laminates containing 3, 5 and 9 layers. It should be noted that the results are presented for five digits. As you can see the number of the layers doesn't have significant effects on the critical load for U-pattern laminates. While, on the X and and O-patterns increase in the number of layers cause to grow and reduce the buckling load, respectively. Indeed, it can be said in X-pattern, the increase in layer number makes the stiffer laminates, whereas, in O-pattern, it causing the laminate to be weaker.

This section regards to investigate the buckling under biaxial loads. In Table 5, critical loads are presented for biaxial loading. By considering the laminates with SSSS, CCCC, CCSS, and CSCS boundary conditions, results are evaluated for various load parameter R which defined as the ratio of X-axis to Y-axis load ($R = N_{xx}^{0}/N_{yy}^{0}$). It is revealed that the influence of variation of load parameter R on the critical load, is more for lower aspect ratio. Furthermore, by comparing the results displayed in the following table with

Table 5 Critical buckling load for various load parameter R

	$\frac{a}{b}$	U-Type			O-Type			X-Type		
		R = 0.5	R = 1	R = 1.5	R = 0.5	R = 1	R = 1.5	R = 0.5	R = 1	R = 1.5
SSSS	0.5	6.9177	4.1509	2.9650	5.1403	3.0844	2.2031	8.6452	5.1877	3.7055
	1	2.1642	1.6232	1.2985	1.6332	1.2249	0.9799	2.6930	2.0198	1.6158
	1.5	1.4352	1.2144	1.0525	1.0686	0.9042	0.7837	1.8005	1.5236	1.3204
CCCC	0.5	16.0461	11.8003	8.4903	12.3920	8.9230	6.4011	19.3406	14.3903	10.3760
	1	5.9081	4.4653	3.5619	4.3533	3.2882	2.6236	7.4099	5.6038	4.4689
	1.5	4.2306	3.5805	3.0702	3.0822	2.6120	2.2445	5.3458	4.5208	3.8705
CCSS	0.5	11.2720	7.1531	5.1048	8.5632	5.3349	3.8027	13.7142	8.8569	6.3227
	1	3.5877	2.7043	2.1594	2.6684	2.0110	1.6059	4.4903	3.3854	2.7030
	1.5	2.4749	2.1024	1.8166	1.8164	1.5446	1.3365	3.1234	2.6516	2.2889
CSCS	0.5	14.9433	10.8832	8.2082	11.5204	8.3850	6.1789	17.9735	13.1600	10.0358
	1	4.4368	3.2045	2.5035	3.2858	2.3717	1.8524	5.5548	4.0148	3.1374
	1.5	2.0729	1.7052	1.4453	1.5335	1.2616	1.0696	2.6061	2.1441	1.8173

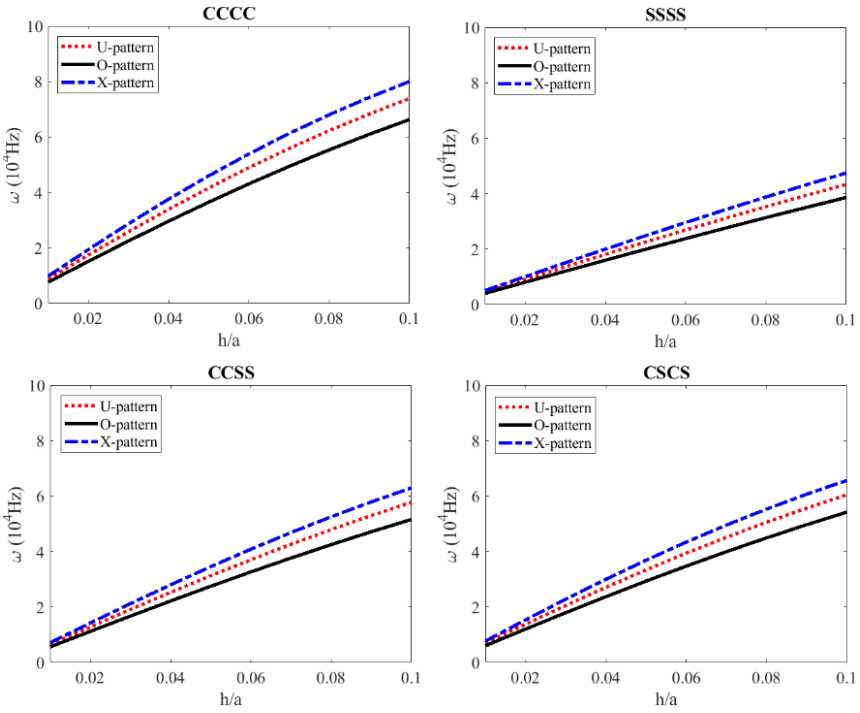

Fig. 6 Varaition of natural frequency with nondimension thickness

the results presented for uniaxial buckling (Fig. 3), as expected, it is known that laminate subjected to biaxial compression mostly provides lower critical load respected to uniaxial compression. It should be noted that if the compression loads ignored from Eq. (14), the explanation of energy function will be dedicated for shear buckling problem. In Fig. 5, critical shear loads are predicted for different conditions. As can be seen, similar to uniaxial loading, in all of the boundary conditions, higher and lower critical buckling loads are corresponded to X and O-templates, respectively. Besides, by comparing Figs. 4 and 5 it is obvious that for the same conditions (same aspect ratio and same laminate configuration), shear loading has been presented larger critical load respected to uniaxial compression. Moreover, by accurate investigation of graphs related to laminates with two free opposite edges (SFSF and CFCF), it is found that for the aspect ratio $a/b > 1.5$, the role of laminate configuration is almost negligible. In the following, free vibration analysis is presented for square laminate. Fig. 6 represents the variation of fundamental frequency with dimensionless thickness ratio (h/a). It is observed that, for all of the boundary conditions, the highest and the lowest frequencies are corresponded to X and O-patterns, respectively. As expected in the laminate with higher h/a, the influence of reinforcement pattern is more severe.

In Table 6, natural frequencies are presented for laminates made from different layers. In this section, the laminate thickness ratio is equal to 0.05. According to this table, one can say in U-pattern, the number of layers does not play a significant role in the laminate frequencies. Whereas for O-pattern (in all of the boundary conditions), increasing the number of layers decreases the frequency and vice versa for X-pattern. In the end, the first forth mode

Table 6 Fundamental frequency (Hz) for various layers number N

	U-Type			O-Type			X-Type		
N	3	5	7	3	5	7	3	5	7
SSSS	22551	22551	22551	20839	19954	19697	24139	24871	25073
CCCC	41600	41600	41600	38271	36492	35971	44608	45986	46364
CCSS	31292	31292	31292	28818	27518	27138	33555	34593	34879
CSCS	33416	33416	33416	30769	29367	28957	35820	36923	37227

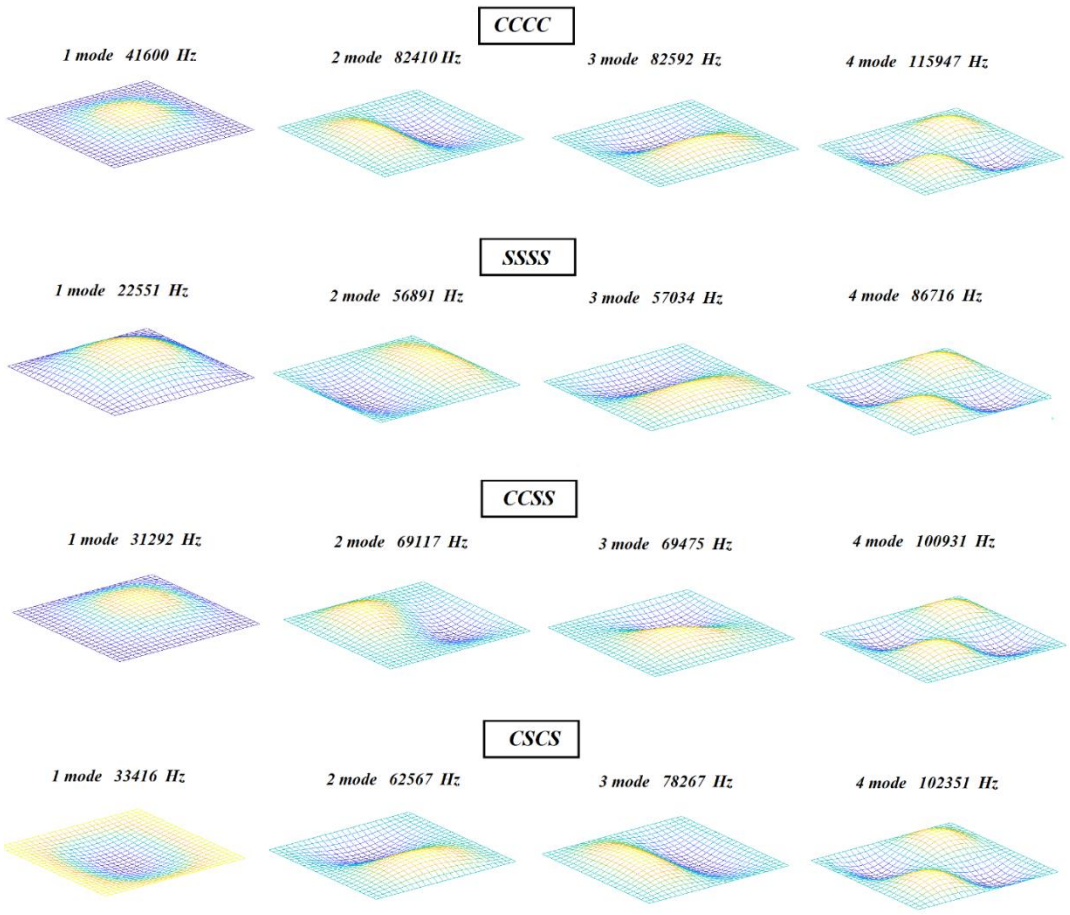

Fig. 7 Laminate mode shapes for various boundary conditions

shapes of lateral vibration of U-pattern square laminates with 0.1 graphene volume fraction are presented in Fig. 7.

6. Conclusions

In the present work, the buckling and free vibration analysis of Graphene/PMMA laminates have been studied. For this aim, the first shear deformation theory is used. Three patterns are used for distribution of Graphene in the laminate. Mechanical properties of the composite are predicted by molecular dynamics simulation. By inserting MD results into the rule of mixture, corrective factors are calibrated, therefore Young's and shear modulus are calculated for each layer. Ritz-Chebyshev method is implemented for the prediction of buckling load. After solving the eigenvalue problem, the critical load and natural frequency are obtained for various geometrically and physically conditions. The results showed that X and O-patterns present the higher and lower buckling loads and natural frequency compared to U-pattern laminates. As well as, it is shown that the number of layers does not have an effect on U-pattern laminates, while it is not right for other patterns.

References

Akgöz, B. and Civalek, Ö. (2017), "A size-dependent beam model for stability of axially loaded carbon nanotubes surrounded by Pasternak elastic foundation", *Compos. Struct.*, **176**, 1028-1038. https://doi.org/10.1016/j.compstruct.2017.06.039

Akgöz, B. and Civalek, Ö. (2018), "Vibrational characteristics of embedded microbeams lying on a two-parameter elastic foundation in thermal environment", *Compos. Part B: Eng.*, **150**, 68-77. https://doi.org/10.1016/j.compositesb.2018.05.049

Alibeigi, B., Tadi Beni, Y. and Mehralian, F. (2018), "On the thermal buckling of magneto-electro-elastic piezoelectric nanobeams", *Eur. Phys. J. Plus*, **133**, 133. https://doi.org/10.1140/epjp/i2018-11954-7

Aydogdu, M. (2014), "On the vibration of aligned carbon nanotube reinforced composite beams", *Adv. Nano Res., Int. J.*, **2**(4), 199-210. https://doi.org/10.12989/ANR.2014.2.4.199

Besseghier, A., Heireche, H., Bousahla, A.A., Tounsi, A. and Benzair, A. (2015), "Nonlinear vibration properties of a zigzag single-walled carbon nanotube embedded in a polymer matrix", *Adv. Nano Res., Int. J.*, **3**(1), 29-37. https://doi.org/10.12989/ANR.2015.3.1.029

Chen, S., Sun, S., Li, C., Pittman, C.U., Lacy, T.E., Hu, S. and Gwaltney, S.R. (2018), "Molecular dynamics simulations of the aggregation behaviour of overlapped graphene sheets in linear aliphatic hydrocarbons", *Molecul. Simul.*, **44**(12), 947-953. https://doi.org/10.1080/08927022.2018.1465569

Dastjerdi, S. and Akgöz, B. (2018), "New static and dynamic analyses of macro and nano FGM plates using exact three-dimensional elasticity in thermal environment", *Compos. Struct.*, **192**, 626-641. https://doi.org/10.1016/j.compstruct.2018.03.058

Ebnali Samani, M. and Tadi Beni, Y. (2018), "Size dependent thermo-mechanical buckling of the flexoelectric nanobeam", *Mater. Res. Express*, **5**(8), 085018. https://doi.org/10.1088/2053-1591/aad2ca

Ebrahimi, F. and Habibi, S. (2017), "Low-velocity impact response of laminated FG-CNT reinforced composite plates in thermal environment", *Adv. Nano Res., Int. J.*, **5**(2), 69-97. https://doi.org/10.12989/anr.2017.5.2.069

Emdadi, M., Mohammadimehr, M. and Navi, B.R. (2019), "Free vibration of an annular sandwich plate with CNTRC facesheets and FG porous cores using Ritz method", *Adv. Nano Res., Int. J.*, **7**(2), 109-123. https://doi.org/10.12989/anr.2019.7.2.109

Fan, Y., Xiang, Y. and Shen, H.-S. (2019), "Nonlinear forced vibration of FG-GRC laminated plates resting on visco-Pasternak foundations", *Compos. Struct.*, **209**, 443-452. https://doi.org/10.1016/j.compstruct.2018.10.084

Ghobadi, A., Tadi Beni, Y. and Golestanian, H. (2019), "Size dependent thermo-electro-mechanical nonlinear bending analysis of flexoelectric nano-plate in the presence of magnetic field", *Int. J. Mech. Sci.*, **152**, 118-137. https://doi.org/10.1016/j.ijmecsci.2018.12.049

Han, Y. and Elliott, J. (2007)," Molecular dynamics simulations of the elastic properties of polymer/carbon nanotube composites", *Computat. Mater. Sci.*, **39**(2), 315-323. https://doi.org/10.1016/j.commatsci.2006.06.011

Huang, B.Z. and Atluri, S.N. (1995), "A simple method to follow post-buckling paths in finite element analysis", *Comput. Struct.*, **57**(3), 477-489. https://doi.org/10.1016/0045-7949(94)00623-B

Jaiganesh, V., Manivannan, S. and Maruthu, B. (2015), "Rapid Prototyping of Polymethyl Methacrylate as Replacement and Support of Spine in Human", *Biomed. Res.*, **26**(4), S62-65.

Jia, L. and Qingsheng, Y. (2009), "Molecular dynamics simulation for mechanical properties of CNT/Polyethylene composites", *J. Phys.: Conference Series*, **188**, 012052. https://doi.org/10.1088/1742-6596/188/1/012052

Jia, W., Li, Z., Wu, Z., Wang, L., Wu, B., Wang, Y., Cao, Y. and Li, J. (2018), "Graphene oxide as a filler to improve the performance of PAN-$LiClO_4$ flexible solid polymer electrolyte", *Solid State Ionics*, **315**, 7-13. https://doi.org/10.1016/j.ssi.2017.11.026

Karimi Zeverdejani, M., Tadi Beni, Y. and Kiani, Y. (2019), "Multi-scale Buckling and Post-buckling analysis of functionally graded Laminated Composite Plates Reinforced by Defective Graphene Sheets", *Int. J. Struct. Stabil. Dyn.*, 2050001 https://doi.org/10.1142/S0219455420500017

Kaushik, B.K. and Majumder, M.K. (2015), "Carbon Nanotube: Properties and Applications", In: *Carbon Nanotube Based VLSI Interconnects: Analysis and Design*, (B.K. Kaushik and M.K. Majumder Eds.), New Delhi: Springer India, pp. 17-37.

Kheibari, F. and Tadi Beni, Y. (2017), "Size dependent electro-mechanical vibration of single-walled piezoelectric nanotubes using thin shell model", *Mater. Des.*, **114**, 572-583. https://doi.org/10.1016/j.matdes.2016.10.041

Kiani, Y. (2017), "Buckling of FG-CNT-reinforced composite plates subjected to parabolic loading", *Acta Mechanica*, **228**(4), 1303-1319. https:10.1007/s00707-016-1781-4

Kiani, Y., Dimitri, R. and Tornabene, F. (2018a), "Free vibration of FG-CNT reinforced composite skew cylindrical shells using the Chebyshev-Ritz formulation", *Compos. Part B: Eng.*, **147**, 169-177. https://doi.org/10.1016/j.compositesb.2018.04.028

Kiani, Y., Dimitri, R. and Tornabene, F. (2018b), "Free vibration study of composite conical panels reinforced with FG-CNTs", *Eng. Struct.*, **172**, 472-482. https://doi.org/10.1016/j.engstruct.2018.06.006

Kocman, M., Pykal, M. and Jurecka, P. (2014), "Electric quadrupole moment of graphene and its effect on intermolecular interactions", *Phys. Chem. Chem. Phys.*, **16**(7), 3144-3152. https://doi.org/10.1039/c3cp54701a

Li, Y., Wang, Q. and Wang, S. (2019), "A review on enhancement of mechanical and tribological properties of polymer composites reinforced by carbon nanotubes and graphene sheet: Molecular dynamics simulations", *Compos. Part B: Eng.*, **160**, 348-361. https://doi.org/10.1016/j.compositesb.2018.12.026

Lin, F., Xiang, Y. and Shen, H.-S. (2017), "Temperature dependent

mechanical properties of graphene reinforced polymer nanocomposites – A molecular dynamics simulation", *Compos. Part B: Eng.*, **111**, 261-269. https://doi.org/10.1016/j.compositesb.2016.12.004

Malekzadeh, P. and Zarei, A.R. (2014), "Free vibration of quadrilateral laminated plates with carbon nanotube reinforced composite layers", *Thin-Wall. Struct.*, **82**, 221-232. https://doi.org/10.1016/j.tws.2014.04.016

Mehralian, F. and Tadi Beni, Y. (2016), "Size-dependent torsional buckling analysis of functionally graded cylindrical shell", *Compos. Part B: Eng.*, **94**, 11-25. https://doi.org/10.1016/j.compositesb.2016.03.048

Mehralian, F., Tadi Beni, Y. and Ansari, R. (2016a), "On the size dependent buckling of anisotropic piezoelectric cylindrical shells under combined axial compression and lateral pressure", *Int. J. Mech. Sci.*, **119**, 155-169. https://doi.org/10.1016/j.ijmecsci.2016.10.006

Mehralian, F., Tadi Beni, Y. and Ansari, R. (2016b), "Size dependent buckling analysis of functionally graded piezoelectric cylindrical nanoshell", *Compos. Struct.*, **152**, 45-61. https://doi.org/10.1016/j.compstruct.2016.05.024

Mirzaei, M. and Kiani, Y. (2016), "Free vibration of functionally graded carbon nanotube reinforced composite cylindrical panels", *Compos. Struct.*, **142**, 45-56. https://doi.org/10.1016/j.compstruct.2015.12.071

Mirzaei, M. and Kiani, Y. (2017), "Isogeometric thermal buckling analysis of temperature dependent FG graphene reinforced laminated plates using NURBS formulation", *Compos. Struct.*, **180**, 606-616. https://doi.org/10.1016/j.compstruct.2017.08.057

Mittal, G., Dhand, V., Rhee, K.Y., Park, S.-J. and Lee, W.R. (2015), "A review on carbon nanotubes and graphene as fillers in reinforced polymer nanocomposites", *J. Ind. Eng. Chem.*, **21**, 11-25. https://doi.org/10.1016/j.jiec.2014.03.022

Mohammadimehr, M., Emdadi, M., Afshari, H. and Rousta Navi, B. (2018), "Bending, buckling and vibration analyses of MSGT microcomposite circular-annular sandwich plate under hydro-thermo-magneto-mechanical loadings using DQM", *Int. J. Smart Nano Mater.*, **9**, 233-260. https://doi.org/10.1080/19475411.2017.1377312

Mohtashami, M. and Tadi Beni, Y. (2019), "Size-Dependent Buckling and Vibrations of Piezoelectric Nanobeam with Finite Element Method", *Iran. J. Sci. Technol., Transact. Civil Eng.*, **43**, 563-576. https://doi.org/10.1007/s40996-018-00229-9

Nemeth, M.P. (1986), "Importance of anisotropy on buckling of compression-loaded symmetric composite plates", *AIAA Journal*, **24**(11), 1831-1835. https://doi.org/10.2514/3.9531

Nguyen-Quang, K., Vo-Duy, T., Dang-Trung, H. and Nguyen-Thoi, T. (2018), "An isogeometric approach for dynamic response of laminated FG-CNT reinforced composite plates integrated with piezoelectric layers", *Comput. Methods Appl. Mech. Eng.*, **332**, 25-46. https://doi.org/10.1016/j.cma.2017.12.010

Ramanathan, T., Stankovich, S., Dikin, D.A., Liu, H., Shen, H., Nguyen, S.T. and Brinson, L.C. (2007), "Graphitic nanofillers in PMMA nanocomposites—An investigation of particle size and dispersion and their influence on nanocomposite properties", *J. Polym. Sci. Part B: Polym. Phys.*, **45**(15), 2097-2112. https://doi.org/10.1002/polb.21187

Reddy, C.D., Rajendran, S. and Liew, K.M. (2005), "Equivalent continuum modeling of graphene sheets", *Int. J. Nanosci.*, **4**(4), 631-636. https://doi.org/10.1142/S0219581X05003528

Rodriguez-Perez, M., Villanueva-Cab, J. and Pal, U. (2017), "Evaluation of thermally and chemically reduced graphene oxide films as counter electrodes on dye-sensitized solar cells", *Adv. Nano Res., Int. J.*, **5**(3), 231-244. https://doi.org/10.12989/anr.2017.5.3.231

Sakhaee-Pour, A. (2009), "Elastic properties of single-layered graphene sheet", *Solid State Commun.*, **149**(1), 91-95. https://doi.org/10.1016/j.ssc.2008.09.050

Sayyad, A.S. and Ghugal, Y.M. (2014), "On the Buckling of Isotropic, Transversely Isotropic and Laminated Composite Rectangular Plates", *Int. J. Struct. Stabil. Dyn.*, **14**, 1450020. https://doi.org/10.1142/S0219455414500205

Shiu, S.-C. and Tsai, J.-L. (2014), "Characterizing thermal and mechanical properties of graphene/epoxy nanocomposites", *Compos. Part B: Eng.*, **56**, 691-697. https://doi.org/10.1016/j.compositesb.2013.09.007

Shen, H.-S. and Xiang, Y. (2018), "Postbuckling of functionally graded graphene-reinforced composite laminated cylindrical shells subjected to external pressure in thermal environments", Thin-Walled Structures, 124, 151-160. https://doi.org/10.1016/j.tws.2017.12.005

Shen, H.-S. and Xiang, Y. (2019), "Torsional postbuckling behavior of FG-GRC laminated cylindrical shells in thermal environments", *Thin-Wall. Struct.*, **135**, 560-574. https://doi.org/10.1016/j.tws.2018.11.025

Shen, H.-S., Lin, F. and Xiang, Y. (2017a), "Nonlinear bending and thermal postbuckling of functionally graded graphene-reinforced composite laminated beams resting on elastic foundations", *Eng. Struct.*, **140**, 89-97. https://doi.org/10.1016/j.engstruct.2017.02.069

Shen, H.-S., Xiang, Y. and Fan, Y. (2017b), "Nonlinear vibration of functionally graded graphene-reinforced composite laminated cylindrical shells in thermal environments", *Compos. Struct.*, **182**, 447-456. https://doi.org/10.1016/j.compstruct.2017.09.010

Shen, H.-S., Xiang, Y., Fan, Y. and Hui, D. (2018), "Nonlinear bending analysis of FG-GRC laminated cylindrical panels on elastic foundations in thermal environments", *Compos. Part B: Eng.*, **141**, 148-157. https://doi.org/10.1016/j.compositesb.2017.12.048

Shojaeian, M. and Tadi Beni, Y. (2015), "Size-dependent electromechanical buckling of functionally graded electrostatic nano-bridges", *Sensors Actuators A: Phys.*, **232**, 49-62. https://doi.org/10.1016/j.sna.2015.04.025

Soleimani, I. and Tadi Beni, Y. (2018), "Vibration analysis of nanotubes based on two-node size dependent axisymmetric shell element", *Arch. Civil Mech. Eng.*, **18**, 1345-1358. https://doi.org/10.1016/j.acme.2018.04.009

Song, M., Yang, J., Kitipornchai, S. and Zhu, W. (2017), "Buckling and postbuckling of biaxially compressed functionally graded multilayer graphene nanoplatelet-reinforced polymer composite plates", *Int. J. Mech. Sci.*, **131-132**, 345-355. https://doi.org/10.1016/j.ijmecsci.2017.07.017

Tadi Beni, Y. (2016), "Size-dependent electromechanical bending, buckling, and free vibration analysis of functionally graded piezoelectric nanobeams", *J. Intel. Mater. Syst. Struct.*, **27**, 2199-2215. https://doi.org/10.1177/1045389X15624798

Tadi Beni, Y. and Mehralian, F. (2017), "Size-dependent torsional buckling of carbon nano-peapods based on the modified couple stress theory", *Int. J. Appl. Mech.*, **9**(2), 1750030. https://doi.org/10.1142/S1758825117500302

Tadi Beni, Y., Mehralian, F. and Razavi, H. (2015), "Free vibration analysis of size-dependent shear deformable functionally graded cylindrical shell on the basis of modified couple stress theory", *Compos. Struct.*, **120**, 65-78. https://doi.org/10.1016/j.compstruct.2014.09.065

Tadi Beni, Y., Karimi Zeverdejani, M. and Mehralian, F. (2017), "Buckling analysis of orthotropic protein microtubules under axial and radial compression based on couple stress theory", *Mathe. Biosci.*, **292**, 18-29. https://doi.org/10.1016/j.mbs.2017.07.002

Tam, M., Yang, Z., Zhao, S. and Yang, L. (2019), "Vibration and buckling characteristics of functionally graded graphene nanoplatelets reinforced composite beams with open edge cracks", *Materials*, **12**, 1412. https://doi.org/10.3390/ma12091412

Van Krevelen, D.W. and Te Nijenhuis, K. (2009), Chapter 13 – "Mechanical Properties of Solid Polymers", In: *Properties of Polymers* (Fourth Edition), (D.W. Van Krevelen and K. Te Nijenhuis Eds.), Elsevier, Amsterdam, Netherlands, pp. 383-503.

Walter, T.R., Bujanda, A.A., Rodriguez-Santiago, V., Yim, J.H., Baeza, J.A. and Pappas, D.D. (2016), "Enhanced Mechanical Performance of Woven Composite Laminates Using Plasma Treated Polymeric Fabrics", In: *Advanced Composites for Aerospace*, *Marine*, *and Land Applications*, (T. Sano, T.S. Srivatsan and M.W. Peretti Eds.), Cham: Springer International Publishing, pp. 231-242.

Zhang, Y. and Park, S.l. (2018), "Influence of the nanoscaled hybrid based on nanodiamond@graphene oxide architecture on the rheological and thermo-physical performances of carboxylated-polymeric composites", *Compos*. *Part A*: *Appl*. *Sci*. *Manuf*., **112**, 356-364. https://doi.org/10.1016/j.compositesa.2018.06.020

Zhang, Y. and Park, S.l. (2019), "Imidazolium-optimized conductive interfaces in multilayer graphene nanoplatelet/epoxy composites for thermal management applications and electroactive devices", *Polymer*, **168**, 53-60. https://doi.org/10.1016/j.polymer.2019.01.086

Zhang, Y., Ge, X., Li, M., Deng, F., Oh, J. and Cho, U. (2018a), "The properties of rice bran carbon/nitrile-butadiene rubber composites fabricated by latex compounding method", *Polym*. *Compos*., **39**(S2), E687-E696. https://doi.org/10.1002/pc.24126

Zhang, Z., Li, Y., Wu, H., Zhang, H., Wu, H., Jiang, S. and Chai, G. (2018b), "Mechanical analysis of functionally graded graphene oxide-reinforced composite beams based on the first-order shear deformation theory", *Mech*. *Adv*. *Mater*. *Struct*., 1-9. https://doi.org/10.1080/15376494.2018.1444216

CC